

# CORONAGRAPH BASED BEAM HALO MONITOR DEVELOPMENT FOR BERLINPRO

Ji-Gwang Hwang\*, Jens Kuszynski, Helmholtz-Zentrum Berlin, Berlin, Germany

## Abstract

For linac based high power electron machines, beam halo induced by nonlinear space charge force and scattering of trapped ions is one of the critical issues on a machine protection system. It causes additional radiation which can be a heat source on a cryogenic system as a result of uncontrolled beam losses. During the last decades, several instruments have been newly developed for measuring the beam halo distribution. The conceptual design and optimization of the coronagraph based halo monitor were performed to measure the beam halo which has  $\sim 10^{-3}$  contrast to the beam core.

## INTRODUCTION

The bERLinPro is ongoing at Helmholtz-Zentrum Berlin (HZB) in order to demonstrate and establish technologies for energy recover linear (ERL) accelerator performance towards a future light source [1, 2]. The superconducting linacs can provide both a low emittance and high average-current electron beams that could produce ultra-brilliant X-rays [3] or drive X-ray free-electron lasers in continuous wave (CW) operation [4]. The bERLinPro will provide electron beams up to 50 MeV in the recirculation loop with several operation modes such as the single pulse mode, bursting mode, and a CW mode [5]. The injector system which consists of the photo-cathode RF gun, booster linac, and merger will provide electron beams with the energy of 6.5 MeV and beam current of 100 mA [6]. The layout is shown in Fig. 1.

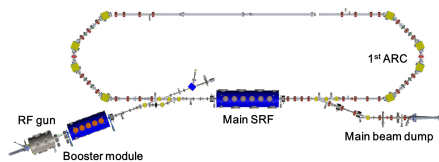


Figure 1: Schematic drawing of bERLinPro.

In the arc section of the re-circulation loop of the bERLinPro, many optical beam diagnostics which are based on synchrotron radiation from dipole magnets will be installed for observing the beam size, coherent synchrotron radiation (CSR) and halo distribution. The coronagraph based halo monitor is a crucial diagnostic for minimizing uncontrolled beam losses due to halo particles by adjusting the optics at the upstream of the arc section. In order to estimate the halo distribution at the exit of the second dipole magnet in the re-circulation loop, the multi-particle tracking simulation with 1 million macro-particles using

the OPAL code [7], which can compute relativistic particles distribution in fully 6-dimensional phase spaces taking into account a space charge force with multiple-components was conducted. The particle distribution is shown in Fig. 2.

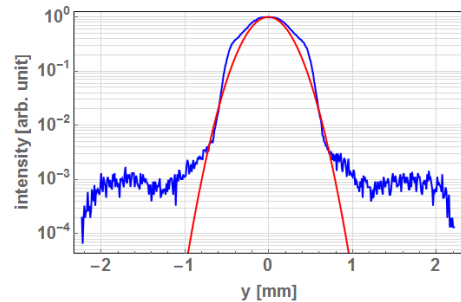


Figure 2: Particle distribution on vertical plane at exit of second dipole magnet in arc section. The red line was calculated by using a Gaussian fitting.

From the calculation result, the beam intensity over  $6\sigma_y$  (RMS beam size),  $\sim 1.28$  mm, is about  $10^{-3}$  contrast to the beam core. The beam distribution in the horizontal plane is widespread and has non-Gaussian distribution due to the dispersion. The coronagraph is aiming for halo observation of  $10^{-3}$  to  $10^{-4}$  contrast to the beam core.

## CORONAGRAPH BASED HALO MONITOR

For the observation of the halo distribution with the contrast of  $10^{-3}$  to  $10^{-4}$  to the beam core, a special technique is required to reduce the background noise because the high intensity light from the beam core produces diffraction fringes with the intensity of  $10^{-2}$  when the image of the beam produced by using an optical lens with a finite aperture. Many techniques are developed [8–10]. The Lyot’s idea for the coronagraph is to install a field lens at the focal plane of an objective lens and to put a mask (Lyot stop) at the focal plane of the field lens to remove the majority of diffraction fringes produced using the re-diffraction optics.

### Optimization of Objective Lens Section

The coronagraph based halo monitor consists of an objective lens (first lens) to produce the real beam image, opaque disk to block the high intensity light from the beam core, field lens (second lens) to produce the re-diffraction fringes, Lyot stop to remove the majority of the diffraction fringes, and a relay lens (third lens) to make the image for a CCD camera (Fig.3). The beam distribution and diffraction fringe at the focal plane of the objective lens with the wavelength

\* ji-gwang.hwang@helmholtz-berlin.de

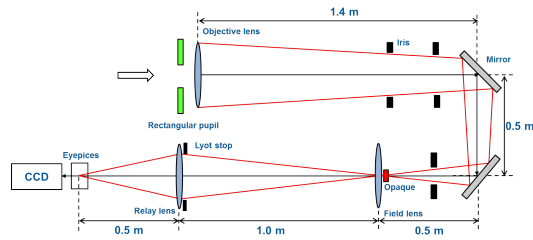


Figure 3: Schematic layout of the designed coronagraph based halo monitor.

of 500 nm, entrance pupil size of 40 mm, and focal length of 2 m are shown in Fig. 4.

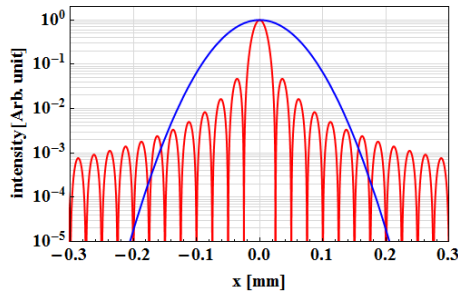


Figure 4: Beam distribution (blue) and diffraction fringe (red) at focal plane of objective lens with wavelength of 500 nm, entrance pupil size of 40 mm, and focal length of 2 m.

The disturbance of the diffracted light  $F(x)$  on the imaging plane of the lens is given by

$$F(x, y) = \frac{1}{i\lambda f} \iint f(\xi, \eta) e^{-\frac{i2\pi(x\xi + y\eta)}{\lambda f}} d\xi d\eta, \quad (1)$$

where  $f(\xi)$  denote the disturbance of the light on the lens entrance, the  $\lambda$  is the wavelength, and  $f$  is the focal length [11].

The distance between the central maximum of the fringes and the first minimum which is called an Airy distance is proportional to  $\sim \lambda f/d$ , where  $d$  is the entrance pupil size. The size of the opaque disk is determined by the beam size and magnification of the objective lens. The magnification of the lens is given by  $f/(s-f)$ , where  $s$  is the distance from the source point to the entrance pupil. For the optimization of the focal length of the objective lens, the relative distance of the Airy distance and beam profile as a function of the focal length of the objective lens was calculated. The values are normalized by the value with the focal length of 1 m. It is shown in Fig. 5.

From the calculation result, the power of the diffraction fringes removed by opaque disk which is defined by the  $6 \times \sigma$  beam size is increased when the entrance pupil size is increased, focal length is increased and wavelength is shorter. The longer focal length is also good to reduce the aberrations. But the entrance pupil size and wavelength are limited by the size of the optical guide and energy of the beam, respectively. In our case, the RMS beam size is about 214  $\mu\text{m}$  and distance from the source point to entrance pupil would be 12 m long. The focal length of the objective lens,

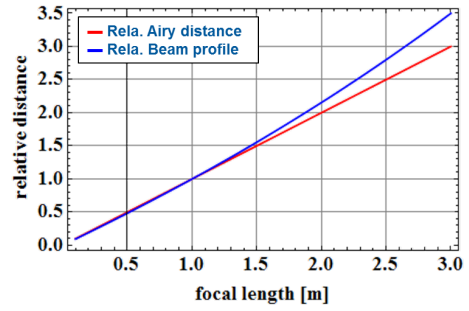


Figure 5: Relative distance of Airy distance and beam profile as a function of focal length of objective lens.

pupil size and wavelength are determined to 2 m long, 40 mm and 500 nm, respectively. The radius of the opaque disk is 257  $\mu\text{m}$ .

### Optimization of Field Lens Section

The re-diffraction system, in which, the field lens is focused on the objective lens aperture, and has an aperture due to central opaque disk. The input disturbance of the light is given by the disturbance of the diffraction pattern of the objective lens. The diffraction of the field lens aperture for an opaque disk is calculated using Babinet's theory [11]. The calculation of the intensity distribution at the focal plane of the field lens with various focal lengths is shown in Fig. 6.

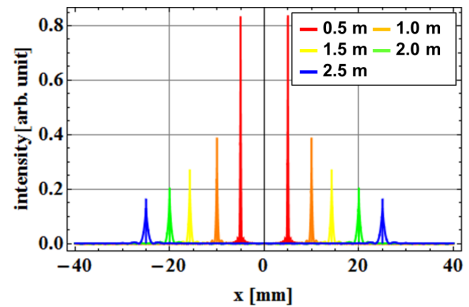


Figure 6: Calculation result of intensity distribution at focal plane of field lens with various focal lengths. The wavelength and focal length of objective lens are 500 nm and 2 m, respectively.

The peak position of the diffraction fringe corresponds to the geometrical image of the aperture edge at the entrance pupil which is determined by the ratio of focal length of objective lens to field lens and entrance pupil. As the focal length of the field lens increases, the distance between two peaks is widens and power distribution spreads out. In our case, the diameter of the relay lens is less than 50 mm and the maximum opening of the Lyot stop is 25 mm. A commercially available achromatic lens with the focal length of 1 m is adopted. The intensity distribution on the focal plane of the field lens with the focal length of 1 m is shown in Fig. 7.

Since the real image of the halo beam is distributed near the vicinity of the re-diffraction peak, the opening of the

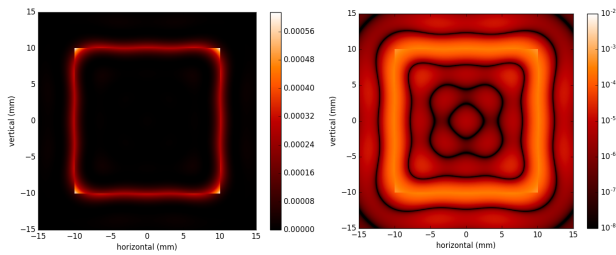


Figure 7: Calculations of linear (left) and log (right) scale intensity distribution on focal plane of re-diffraction system.

Lyot stop is finely adjustable from 5 mm to 20 mm. The circular type Lyot stop is adopted to prevent the invasion of the power from the corner of the re-diffraction fringes which contains the maximum power.

### Relay System and Background Level

The diffraction fringes created in the third stage, the relay system, is calculated using the diffraction integral with the Lyot stop as an entrance pupil on the image point of the relay lens. The diameter of the relay lens is set to 50 mm because the opening of the Lyot stop is adjustable up to 20 mm. A commercially available achromatic lens with the focal length of 0.5 m is adopted. Since the transverse magnification of relay system is not enough, the projection lens (eyepices) is required in the front of the CCD camera. The intensity distribution of the diffraction pattern on the imaging plane of the relay lens with the opening of the Lyot stop of 8 mm is shown in Fig. 8.

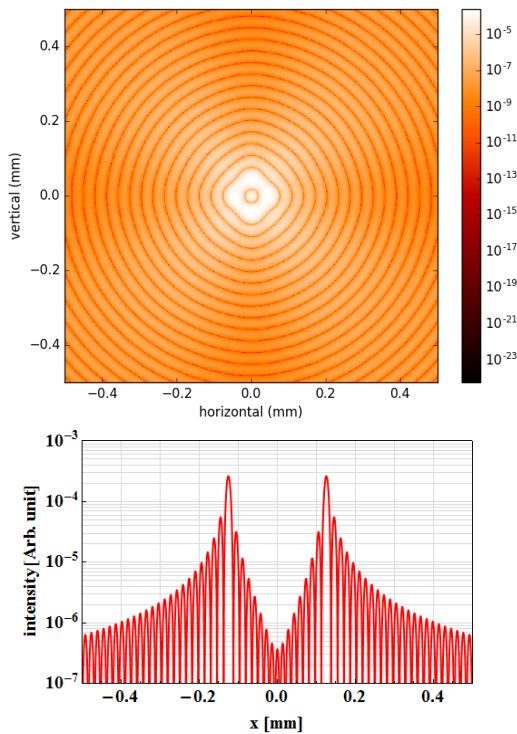


Figure 8: Intensity distribution of diffraction pattern on imaging plane of relay lens with Lyot stop opening of 8 mm.

As shown in the calculation result, the diffraction pattern due to the relay lens has a relative peak intensity of about  $2.5 \times 10^{-4}$ . In the range of  $10^{-4}$  contrast, the polishing quality of the lens should be better than  $200 \mu\text{m}$  because the background noise from the Mie-scattering effect due to the dig and scratch on the lens surface is  $3 \times 10^{-4}$  for a  $200 \mu\text{m}$  dig [11]. A reflection free structure is considered for the first stage, the objective lens section, to prevent the effect of the background light. Several baffle slits are inserted in the first stage.

### ACKNOWLEDGEMENT

The particle distribution shown in Fig. 2 was provided by Bettina Kuske in HZB. The authors wish to thank Prof. T. Mitsuhashi in KEK for his valuable discussion and advice. This work was supported by the German Bundesministerium für Bildung und Forschung, Land Berlin and grants of Helmholtz Association.

### CONCLUSION

The design study of the coronagraph based halo monitor was performed to observe the halo distribution with  $\sim 10^{-3}$  contrast to the beam core. The size of the entrance pupil, focal length of the objective lens and focal lens, and opening of the Lyot stop is optimized. The diffraction pattern by the relay lens has the peak intensity of about  $2.5 \times 10^{-4}$ . The polishing quality of the lens should be better than  $200 \mu\text{m}$  to reduce the background noise from the Mie-scattering effect. The experiment and commissioning of the designed halo monitor system will be performed in Metrology Light Source [12].

### REFERENCES

- [1] B. Kuske, N. Paulick, A. Jankowiak, J. Knobloch eds. *bERLinPro Conceptual design report* (2012), [https://www.helmholtz-berlin.de/media/media/grossgeraete/beschleunigerphysik/berlinpro\\_MAB/BPro\\_in\\_detail/Publications/berLinPro\\_CDR.pdf](https://www.helmholtz-berlin.de/media/media/grossgeraete/beschleunigerphysik/berlinpro_MAB/BPro_in_detail/Publications/berLinPro_CDR.pdf).
- [2] A. Jankowiak, *et al.*, *Proceedings of LINAC10*, Tsukuba, Japan, TUP007 (2010).
- [3] G. H. Hoffstaetter, S. Gruner, M. Tigner, eds., *Cornell ERL Project Definition Design Report* (2011), <http://www.classe.cornell.edu/Research/ERL/PDDR.html>.
- [4] J. Galayda, *Proceedings of IPAC14*, Dresden, Germany, p. 935 (2014).
- [5] M. Abo-Bakr, *et al.*, *Proceedings of IPAC 2015*, Richmond, USA, TUPWA018 (2015).
- [6] M. Abo-Bakr, *et al.*, *Proceedings of IPAC 2016*, Busan, Korea, TUPOW034 (2016).
- [7] OPAL website, [https://www.desy.de/~mpyflo/Astra\\_documentation/](https://www.desy.de/~mpyflo/Astra_documentation/).
- [8] T. Mitsuhashi, *Proceedings of DIPAC 2005*, Lyon, France, ITMM03 (2005).
- [9] H. D. Zhang, *et al.*, *Phys. Rev. ST Accel. Beams*, **15**, 072803 (2012).

- [10] Hideki Aoyagi, *et al.*, *Phys. Rev. ST Accel. Beams*, **15**, 022801 (2012).      [12] J. Feikes, *et al.*, *Phys. Rev. ST Accel. Beams*, **14**, 030705 (2011).
- [11] T. Mitsuhashi, *et al.*, *Proceedings of IBIC2015*, TUCLA03 (2015).